AD-A091 386 INDIANA UNIV AT BLOOMINGTON DEPT OF CHEMISTRY F/G 20/2
EFFECTS OF GAS COMPOSITION AND FLAME SHEATHING ON THE SPATIAL V--ETC(U)
OCT 80 R E RUSSO, G M HIEFTJE N00014-76-C-0838
UNCLASSIFIED TR-29 NL

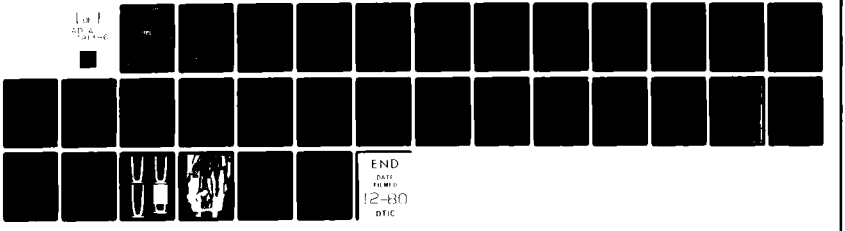

END
DATE FILMED
12-80
DTIC

UNCLASSIFIED

SECURITY CLASSIFICATION OF THIS PAGE (When Data Entered)

REPORT DOCUMENTATION PAGE	READ INSTRUCTIONS BEFORE COMPLETING FORM
1. REPORT NUMBER: TWENTY-NINE	2. GOVT ACCESSION NO.: AD-A091386
3. RECIPIENT'S CATALOG NUMBER:	
4. TITLE (and Subtitle): Effects of Gas Composition and Flame Sheathing on the Spatial Velocity Profiles of Laminar Analytical Acetylene Flames	5. TYPE OF REPORT & PERIOD COVERED: Interim Technical Report
	6. PERFORMING ORG. REPORT NUMBER: 36
7. AUTHOR(s): R. E. Russo and G. M. Hieftje	8. CONTRACT OR GRANT NUMBER(s): N-14-C-0838
9. PERFORMING ORGANIZATION NAME AND ADDRESS: Department of Chemistry, Indiana University, Bloomington, Indiana 47405	10. PROGRAM ELEMENT, PROJECT, TASK AREA & WORK UNIT NUMBERS: NR 51-622
11. CONTROLLING OFFICE NAME AND ADDRESS: Office of Naval Research, Washington, D.C.	12. REPORT DATE: October 2, 1980
	13. NUMBER OF PAGES:
14. MONITORING AGENCY NAME & ADDRESS (if different from Controlling Office)	15. SECURITY CLASS. (of this report): UNCLASSIFIED
	15a. DECLASSIFICATION/DOWNGRADING SCHEDULE

LEVEL II

16. DISTRIBUTION STATEMENT (of this Report)

Approved for public release; distribution unlimited

DTIC ELECTE NOV 6 1980 S C D

17. DISTRIBUTION STATEMENT (of the abstract entered in Block 20, if different from Report)

18. SUPPLEMENTARY NOTES

Prepared for publication in SPECTROCHIMICA ACTA, PART B

19. KEY WORDS (Continue on reverse side if necessary and identify by block number)

20. ABSTRACT (Continue on reverse side if necessary and identify by block number)

A recently developed technique has been empolyed to map the spatial rise velocity profiles (horizontal and vertical) of commonly used laminar analytical flames and to determine the influence on the profiles of fuel-to-oxidant ratio and the presence of a flame sheath. The rise velocities for fuel-rich, lean, and stoichiometric flames were found to differ substantially, the entire profile being greatest for the fuel-rich condition and lowest for the fuel-lean flame. In addition, the change in rise velocity with the addition of a solid (quartz tube) or gas (N_2) sheath was studied. The flowing sheath, at several different

DD FORM 1 JAN 73 1473 EDITION OF 1 NOV 65 IS OBSOLETE S/N 0102-014-6601

UNCLASSIFIED

SECURITY CLASSIFICATION OF THIS PAGE (When Data Entered)

20. Abstract (continued)

flow rates, affected each rise velocity profile principally by altering atmospheric entrainment and thereby changing secondary combustion in the flame. In contrast, a solid quartz tube used as a sheath produces an additional increase in the entire velocity profile of each flame, since it constrains gas expansion to the direction of flame propagation. The degree to which the velocity of each flame is affected by a sheath is strongly influenced by fuel-to-oxidant ratio.

(15) N00014-76-C-0838

OFFICE OF NAVAL RESEARCH

Contract N14-76-C-0838

Task No. NR 051 -622

(14) TR-29, 36

(9) TECHNICAL REPORT NO. 29

(6) EFFECTS OF GAS COMPOSITION AND FLAME SHEATHING ON THE SPATIAL VELOCITY PROFILES OF LAMINAR ANALYTICAL ACETYLENE FLAMES.

by

(10) R. E. Russo and G. M. Hieftje

Prepared for Publication

in

SPECTROCHIMICA ACTA, PART B

Indiana University

Department of Chemistry

Bloomington, Indiana 47405

(11) 2 Oct 80

(12) 32

176685

BRIEF

A new technique is used to spatially map the velocity of air-acetylene and nitrous oxide-acetylene flames. The effects of fuel-to-oxidant ratio and flame sheath on the rise velocity are presented.

ABSTRACT

A recently developed technique has been employed to map the spatial rise velocity profiles (horizontal and vertical) of commonly used laminar analytical flames and to determine the influence on the profiles of fuel-to-oxidant ratio and the presence of a flame sheath. The rise velocities for fuel-rich, lean, and stoichiometric flames were found to differ substantially, the entire profile being greatest for the fuel-rich condition and lowest for the fuel-lean flame. In addition, the change in rise velocity with the addition of a solid (quartz tube) or gas (N_2) sheath was studied. The flowing sheath, at several different flow rates, affected each rise velocity profile principally by altering atmospheric entrainment and thereby changing secondary combustion in the flame. In contrast, a solid quartz tube used as a sheath produces an additional increase in the entire velocity profile of each flame, since it constrains gas expansion to the direction of flame propagation. The degree to which the velocity of each flame is affected by a sheath is strongly influenced by fuel-to-oxidant ratio.

INTRODUCTION

Analytical flame rise velocity is important from both a practical and fundamental standpoint. In a practical sense, the flame rise velocity governs the amount of time droplets or desolvated particles have to release their vapor-phase products and the period the vapor products spend in the spectrometric measurement region. Therefore, analytical sensitivity and matrix interferences are affected by the rise velocity. In fundamental studies (1-3), the rise velocity acts to spatially separate the events which transpire in the atom formation process. If the spatial rise velocity is known, measurements made as a function of height in the flame can be simply related to time, and the rates of various atomization events can be determined.

Several methods have been devised for measurement of flame rise velocities (4-6). However, each of the methods has its drawbacks. For example, the commonly used particle-track method (4) relies on the assumption that glowing particles of aluminum or other metals travel at the same velocity as the flame gases. Certainly, there is an error due to gravitational attraction acting on these heavy particles. More importantly, detection for this method generally requires photographic analysis of the glowing particle tracks; an error is thereby introduced by the indistinct ends of the incandescent line segments that are photographed. Also, fine spatial resolution is not possible with the particle track method, and a large distribution in flame rise velocities has been measured with the technique. A critical evaluation of this method has been presented by Borgers, et al. (7).

Laser doppler velocimetry, another common method for measuring flame rise velocity, offers good spatial resolution (6), but requires rather complicated and expensive instrumentation.

The method used in the present study to measure flame rise velocity has been described elsewhere (8) and will only briefly be explained here. In this method, a droplet generator (9,10) is used to inject uniform droplets into the flame; when desolvated and vaporized, the droplets each yield a cloud of free atoms which travels with the flame gases. Earlier studies (11) have shown that the droplets themselves, and therefore the atoms they yield, travel at a velocity indistinguishable from that of the flame. Spectrometric detection of the time it takes the atoms to pass two well-defined locations in the flame then gives a direct measure of the rise velocity.

There are several advantages of this measurement technique. First, the method relies upon vapor-phase atoms as a probe and therefore avoids the errors caused by gravitational attraction of heavy particles. Secondly, good spatial resolution is available, which allows one to completely characterize the rise velocity profile. Finally, the technique is very inexpensive to implement and relatively simple to operate.

In the present study, this new method was used to record complete maps (profiles) of the air-acetylene flame at several different fuel-to-oxidant ratios. Variations in the flame rise velocity profiles as different sheaths (N_2 and quartz tube) are incorporated around the flame were also studied. In addition, the radial velocity profile for a nitrous oxide-acetylene flame is included.

EXPERIMENTAL

The experimental system employed in these studies has been detailed in several previous papers (3, 8, 11) and a schematic diagram of the detection system incorporating the double horizontal slit system is portrayed in Figure 1 of reference 3 or 11. Droplets were introduced into the flame at rates between 1-2 KHz and were approximately 50 μm diameter. A Meker-type burner, used to support both the air-acetylene and nitrous-oxide-acetylene flames, was mounted on a translation device which allowed three-dimensional spatial resolution. A constant air flow rate of 16.2 L/min was employed for all air-acetylene flames. The acetylene flow was set at 1.60 L/min (F/O = 0.10), 2.15 L/min (F/O = 0.13), and 2.70 L/min (F/O = 0.17) for the fuel-lean, stoichiometric and fuel-rich conditions, respectively. Nitrogen flows of either 2.30 L/min or 3.80 L/min were used when the flowing flame sheath was employed; the solid sheath consisted of a quartz tube 3.5 cm i.d. x 35 cm high.

The physical dimensions and structure of the flames were examined by Schlieren photography. The experimental arrangement is similar to that of Saturday (12) except for the light source which is here a point source arc lamp (Ionics Inc., Watertown, MA). An exposure time of one millisecond was used for all photographs. With this exposure, most transient variations or perturbations in the flame structure should be resolved (13).

RESULTS AND DISCUSSION

Radial and Vertical Flame Velocity Profiles.

The radial velocity profile of a nitrous-oxide-acetylene flame under approximately stoichiometric conditions is shown in figure 1 (see Figure 2 of reference 14 for a similar profile of the air-acetylene flame). This profile was taken approximately 6 cm above the burner top. This distance is the least possible with the present measurement method because of the relatively high velocity of the nitrous-oxide-acetylene flame and the amount of time required for the large droplets ($\approx$ 50 μm) used here to desolvate and vaporize. The asterisks in Figure 1 represent the average rise velocity measured at each burner location; the error bars represent the 95% confidence limits and show the overall error in the measurement technique to be about 5%. This error is due mainly to slight fluctuations in the droplet's point of entry into the flame, caused by surrounding air currents. The resulting instability is manifested mostly as a laterally-moving vapor cloud. Fortunately, this lateral movement is small compared to the incremental translation steps of the burner.

The dotted line in Figure 1 is obtained from a second-order polynomial fit to the data. Not surprisingly, a computer program designed to choose the best order for the polynomial consistently chose second order for these data with a correlation coefficient of 99% or better.

According to Figure 1, there is an approximately 40% decrease in the rise velocity measured at the edge relative to the center of the flame. However, the limits of Figure 1 do not extend completely to the edge of the flame; the luminous flame boundary is at least 1 mm beyond the region shown in the plot, as determined by photographic observation of the flame and vapor cloud. Therefore, the actual decrease in velocity across the entire

luminous body of the flame will be greater than the measured 40%. For the laminar flame system studied here, the velocity is lowest at the edge because of air drag, cooling, and dilution of the gases. In the center of the flame, the velocity is enhanced by the change in preheating of the flame gases reaching this point (15).

Figure 2 shows the vertical velocity profiles for a stoichiometric air-acetylene flame measured both in the radial center of the flame, and also 2 mm from the flame edge. Note that the greatest velocity is only approximately 10 m/s for the air-acetylene flame, compared to about 16 m/s for the N_2O-acetylene flame. This difference can be attributed mostly to the lower temperature of the air-supported flame; its unburned gas flow velocity from the burner ports is actually greater than that for the nitrous-oxide/acetylene flame.

In the radial center of the air-acetylene flame (cf. Fig. 2A), the velocity decreases only 4% over the observed 9 cm vertical distance. However, the velocity changes at the flame edge (cf. Fig. 2B) by more than 8%. It is reasonable that the flame edge would experience a greater velocity decrease than the center, simply because dilution and cooling of the gases is greater there. Also, the effect of atmospheric drag is more prominent at the flame edge than in the center.

Effect of Fuel-to-Oxidant Ratio

Visually, changes in the fuel-to-oxidant ratio are manifested principally as changes in the physical dimensions and stability of the air-acetylene flame. In particular, the fuel-lean flame appears thinner and more feeble than the relatively bulky, stable fuel-rich flame. These visual characteristics are supported by changes in the rise velocity for each flame condition.

Figure 3 shows velocity profiles for fuel-lean (curve A, F/O = 0.10), stoichiometric (curve B, F/O = 0.13) and fuel-rich (curve C, F/O = 0.17) air-acetylene flames. Each velocity profile was measured at approximately 4 cm above the burner top. Only the second-order polynomial fitted to each set of data are plotted for clarity; all polynomials show $\geq$ 99% correlation to the measured profiles. The velocity profiles for the fuel-rich and fuel-lean flames have been corrected to account for their differences in total flow of unburnt gases, compared to the stoichiometric flame flow. In particular, both the fuel-rich and fuel-lean flames represent a 25% change in the acetylene flow compared to that in the stoichiometric flame. The oxidant flow is the same in all three cases.

From Figure 3, the fuel-lean flame is approximately 13% smaller in diameter than the stoichiometric flame, whereas the fuel-rich flame is approximately 7% wider. These differences in flame width are primarily due to the amount of secondary combustion for each flame condition. The fuel-rich flame also shows the greatest overall velocity primarily because of the greater degree of secondary combustion which it enjoys over the other two flames. Significantly, the greater velocity of the fuel-rich flame cannot be attributed to a higher temperature; in fact, its measured line-reversal temperature is less than that of the stoichiometric flame. The temperature of the fuel-lean flame is also somewhat lower than that of the stoichiometric flame and is partially responsible for its lower velocity profile. The fuel-lean flame shows the "flattest" horizontal profile of the three flame conditions, primarily a result of its limited capacity for secondary combustion.

Effect of Flame Sheath

Many studies employ either a solid or flowing-gas sheath around the flame. For example, an argon sheath has been found to reduce quenching effects in atomic fluorescence and nitrogen sheaths are commonly employed to increase flame stability (16-19). In addition, a quartz tube has been found to increase stability and decrease temperature gradients in the flame (20). In general, the sheath serves two desirable functions: it stabilizes the flame by providing a barrier against external disturbances and it helps to prevent foreign, atmospheric-born contaminants from entering the flame (20). It has also been suggested that the quartz tube protects the flame from "swirls" in the surrounding atmosphere, so that the flame can flow in a more nearly laminar fashion (20).

The effect of a quartz tube on flame velocity is suggested in the photographs of Figure 4. In Figure 4A, a stoichiometric air-acetylene flame burns freely into the atmosphere. In contrast, Figure 4B shows the same flame with a quartz tube placed around it. Clearly the sheath alters dramatically the physical dimensions of the flame. It appears that flame width and "stiffness" are both affected by a flame sheath (the physical changes to the flame when a flowing gas (N_2) sheath is employed are not as marked as with the quartz tube but are still apparent).

Let us now quantitatively evaluate the effects of flowing-gas and quartz sheaths by examining rise velocity profiles. Again, only the "fitted" second-order polynomial for each profile ($\geq$ 99% correlation coefficient) will be shown.

STOICHIOMETRIC FLAME. Figure 5 confirms that rise velocity is strongly affected by a flame sheath. Curve 5A shows the velocity profile for the stoichiometric flame (cf. Fig. 3B) burning freely into the atmosphere. Curves B and C are the profiles obtained when the flowing N_2 sheath is used at flows of 2.3 L/min and 3.8 L/min, respectively. The flowing sheath is seen to increase substantially the rise velocity at the edges of the flame ($\approx$ 15%) with no experimentally measurable effect in the center region.

It is not surprising that an increase in velocity would result from the addition of the flowing gas sheath. The sheath offers a heated, flowing boundary to the burning flame gases, resulting in less atmospheric drag and heat loss. Moreover, because of the laminarity of the flame, the radial center is affected less by heat loss and drag than is the flame edge. The similarity between the two profiles with different nitrogen flows suggests that reduced heat loss is the dominant reason for enhanced flame-edge velocity; reduced air drag would be more strongly influenced by changes in sheath gas flow rates.

As Figure 5D shows, the entire rise velocity profile is increased markedly when a quartz tube surrounds the flame. There is an approximate 38% increase in velocity at the flame edge and about a 7% increase in the radial center. This overall increase is a result of several factors. Primarily, the flame is constrained to burn in a reduced volume which is defined by the dimensions of the quartz tube. Gas expansion during secondary combustion, which is normally isotropic, is largely restricted to the vertical direction, resulting in an increased overall velocity profile. Also, the gases are ex-

panding and burning in a confined region which is considerably hotter than the ambient atmosphere, reducing cooling and dilution of the gases at the edges of the flame. As a result, a greater fractional velocity increase occurs at the edge of the flame than at its center.

Fuel-Rich Flame. Figure 6 shows the velocity profiles of a fuel-rich air-acetylene flame with the same nitrogen flow conditions and quartz tube used with the stoichiometric mixture (cf. Figure 5). In contrast to the stoichiometric flame, the fuel-rich flame experiences a reduction in velocity when the nitrogen sheath (cf. Figures 6B and 6C) is added. Significantly, the profiles of the N_2-sheathed fuel-rich flame (Figures 6B and 6C) are essentially the same as those for the nitrogen-sheathed stoichiometric flame (Figures 5B and 5C). From this result, it appears that the N_2 sheath acts to delay (or retard) the onset of secondary combustion by shielding the flame from atmospheric oxygen. It is not unexpected that the fuel-rich flame, in the absence of secondary combustion, approximates the stoichiometric flame conditions.

A quartz tube placed around the fuel-rich flame is again found to increase the entire velocity profile. However, unlike for the stoichiometric flame, the increase is greatest in the flame center. As before, the overall increase is due to the fixed volume and hotter walls of the confining tube. However, the greater increase in the center compared to the edges is probably a result of reduced air entrainment and a consequent reduction in secondary combustion at the flame edge.

Fuel-Lean Flame. For the fuel-lean flame (cf. Figure 7), a nitrogen sheath is found to have no appreciable effect on the rise velocity profile.

It is proposed here that this independence exists because the nitrogen sheath flows beyond the boundary of the fuel-lean flame. As evident from Figure 3, the fuel-lean flame has a radius of only 6.5 mm and is narrower than either the fuel-rich or stoichiometric flame. However, the burner holes which form the sheath ports are positioned approximately 8.5 mm out from the burner center. Therefore, there is about a 2 mm void between the flame edge and the flowing N_2 sheath.

As with the stoichiometric flame, a quartz tube sheath increases the velocity of the fuel-lean flame more at the edges than in the center. Therefore, for flame conditions in which secondary combustion is not influential, the quartz tube serves primarily to reduce atmospheric drag and heat loss. The magnitude of the velocity increase is less for the fuel-lean than for the stoichiometric flame probably because of the smaller diameter of the former flame.

Schlieren Studies

Schlieren photography was used to study physical changes in the flame's structure caused by the different sheaths. Figure 8 shows Schlieren photographs of the fuel-rich air-acetylene flame; remarkably, little structure (turbulence) is observed, indicating the high degree of laminarity of the flame. Figure 8A shows the unsheathed flame; Figures 8B and 8C represent the same flame with the nitrogen sheath added at 2.3 and 3.8 L/min, respectively, and Figure 8D shows the quartz-sheathed flame.

Clearly, none of the sheaths upset the laminarity of the flame, although slight physical changes appear in the flame structure near the pri-

mary combustion region. Specifically, in Figure 8B, horizontal gas expansion and secondary combustion appear to be restricted directly above the burner top. The effect is even more evident in Figure 8C where the narrow region at the flame base extends farther from the burner top. Apparently, the flowing nitrogen sheath boundary is strong enough to control the burning conditions for a substantial distance. This result can be correlated with the measured decrease in the velocity of the fuel-rich flame (cf. Figure 6). Gas expansion due to secondary combustion is delayed because of the strong shielding effect of the N_2 sheath.

Figure 8D shows the same fuel-rich flame with the quartz tube placed approximately one centimeter above the burner top. It is impossible to observe the flame structure inside the tube because of the tube curvature. However, the flame appears to taper as it enters the tube, indicating a "chimney" effect. This constriction of the flame gases is partially responsible for the observed increase in rise velocity (cf. Figure 6D). Again, the primary reasons for increased velocity are believed to be the reduced volume and hot walls of the quartz tube.

Figure 9 shows the effect of excessively high nitrogen sheath flow. This Schlieren photograph is for the same fuel-rich flame shown in Figure 8 except that the nitrogen sheath flow rate has been increased to 7 L/min. Obviously, the high sheath flow has generated substantial turbulence throughout most of the flame. Figure 9 also indicates that the lack of structure in the photographs of Figure 8 is not an experimental artifact, but rather indicates a high degree of laminarity. In addition, this figure dramatizes

the effect of inhibiting the secondary combustion process. The width of the flame is confined to the boundaries defined by the nitrogen sheath for some distance above the burner top. This situation approaches that of the so-called separated flame (21). Separated flames have found some utility in atomic spectroscopy, but have not become widely accepted because of their large gas consumption and increased turbulence.

Schlieren photographs were also recorded for the other two flame gas compositions studied in this paper (stoichiometric and fuel-lean); similar results were observed for the stoichiometric flame as seen in Figure 8. However, the fuel-lean flame was not significantly affected by the N_2 sheaths, supporting the contention that the sheath flows beyond the flame boundary.

CONCLUSION

The rise velocity of an acetylene flame is found to be strongly affected by changes in both gas composition and flame environment. From the changes observed in the velocity profiles, it appears that a flame sheath not only acts to stabilize the flame, as previously believed, but also substantially affects burning parameters. Changes in the fuel-to-oxidant ratio alter the influence of a flame sheath, with fuel-lean flames being affected least by the presence of either a flowing gas or solid (quartz tube) sheath.

ACKNOWLEDGEMENTS

Supported in part by the Office of Naval Research, by the Public Health Service through grant GM 19704, and by the National Science Foundation through grant CHE 77-22152.

REFERENCES

1. N. C. Clampitt and G. M. Hieftje, Anal. Chem., 44, 1211 (1972).
2. G. J. Bastiaans and G. M. Hieftje, Anal. Chem., 46, 901 (1974).
3. C. B. Boss and G. M. Hieftje, Proc. XX Colloqiuum Spectroscopicum Internationale and 7th International Conference on Atomic Spectroscopy, Invited Lectures I, Státní Pedagogické Nakladatelství, 1977, p. 113.
4. C. Th. J. Alkemade, Ph.D. Thesis, University of Utrecht, 1954.
5. G. Cox, Combust. Flame, 28, 155 (1977).
6. R. J. Baker, P. Hutchinson, and J. H. Whiteclaw, Combust. Flame, 23, 57 (1974).
7. A. J. Borgers, M. J. Jongerius, and Tj. Hollander, Appl. Spectrosc., 34, 46 (1980).
8. C. B. Boss and G. M. Hieftje, Appl. Spectrosc., 32, 377 (1978).
9. G. M. Hieftje and H. V. Malmstadt, Anal. Chem., 40, 1860 (1968).
10. G. M. Hieftje and H. V. Malmstadt, Anal. Chem., 41, 1735 (1969).
11. C. B. Boss, Ph.D. Thesis, Indiana University, 1977.
12. K. A. Saturday, Ph.D. Thesis, Indiana University, 1979.
13. A. G. Gaydon and H. G. Wolfhard, in "Flames, Their Structure Radiation and Temperature," 4th Edition, Chapman and Hall Ltd., London, 1979.
14. R. E. Russo and G. M. Hieftje, Anal. Chim. Acta, (in press, 1980).
15. E. Pungor, in "Flame Photometry Theory", R. A. Chalmers, ed., Van Nostrand, Princeton, N.J., 1967, Ch. 1.

16. D. R. Jenkins, Spectrochim. Acta, Part B, 25, 47 (1970).

17. J. D. Winefordner and R. C. Elser, Anal. Chem., 43(4), 25A (1971).

18. P. J. Slevin, V. I. Muscat, and T. J. Vickers, Appl. Spectrosc., 26, 296 (1972).

19. D. J. Johnson and J. D. Winefordner, Anal. Chem., 48, 341 (1976).

20. G. M. Hieftje and R. I. Bystroff, Spectrochim. Acta, Part B, 30, 187 (1975).

21. R. F. Browner and D. C. Manning, Anal. Chem., 44, 843 (1972).

FIGURE CAPTIONS

Figure 1. Radial velocity profile of a nitrous oxide-acetylene flame. * ≡ measured velocity. Dotted line obtained through second-order curve fit with ≥ 99% correlation. Error bars represent 95% confidence limits.

Figure 2. Vertical velocity profiles for air-acetylene flame. A ≡ velocity measured in the radial center of the flame. B ≡ the velocity measured 2 mm from the flame edge. Error bars represent 95% confidence limits.

Figure 3. Radial velocity profiles of air-acetylene flames with different fuel-to-oxidant ratios. Curve A, F/O = 0.10 curve B, F/O = 0.13, and curve C, F/O = 0.17. Curves obtained from second-order polynomial fit to measured data for each flame condition.

Figure 4. Photographs of the air-acetylene flame without (A) and with (B) a solid flame sheath (quartz tube). Streak in each flame results from the emission of Na droplets introduced using a droplet generator.

Figure 5. Rise velocity profiles of a stoichiometric (F/O = 0.13) air-acetylene flame. Curve A, no sheath; Curve B, flowing

nitrogen sheath at 2.3 L/min; Curve C, flowing nitrogen sheath at 3.8 L/min; and Curve D, quartz tube used as flame sheath.

Figure 6. Rise velocity profiles of a fuel-rich (F/O = 0.17) air-acetylene flame. Curve A, no sheath; Curve B, flowing N_2 sheath at 2.3 L/min; Curve C, flowing N_2 sheath at 3.8 L/min; and Curve D, quartz tube used as flame sheath.

Figure 7. Rise velocity profiles of a fuel-lean (F/O = 0.10) air-acetylene flame. Curve A, no sheath; Curve B, N_2 sheath = 2.3 L/min; Curve C, N_2 sheath = 3.8 L/min, and Curve D, quartz tube used as sheath.

Figure 8. Schlieren photographs of a fuel-rich (F/O = 0.17) air-acetylene flame. Curve A, flame burning freely into atmosphere; no sheath; Curve B, N_2 sheath = 2.3 L/min; Curve C, N_2 sheath = 3.8 L/min; and Curve D, quartz tube placed 1 cm above the burner top.

Figure 9. Schlieren photograph of a fuel-rich (F/O = .17) air-acetylene flame with a N_2 sheath of 7 L/min. Flame is separated at base and very turbulent.

Fig. 1

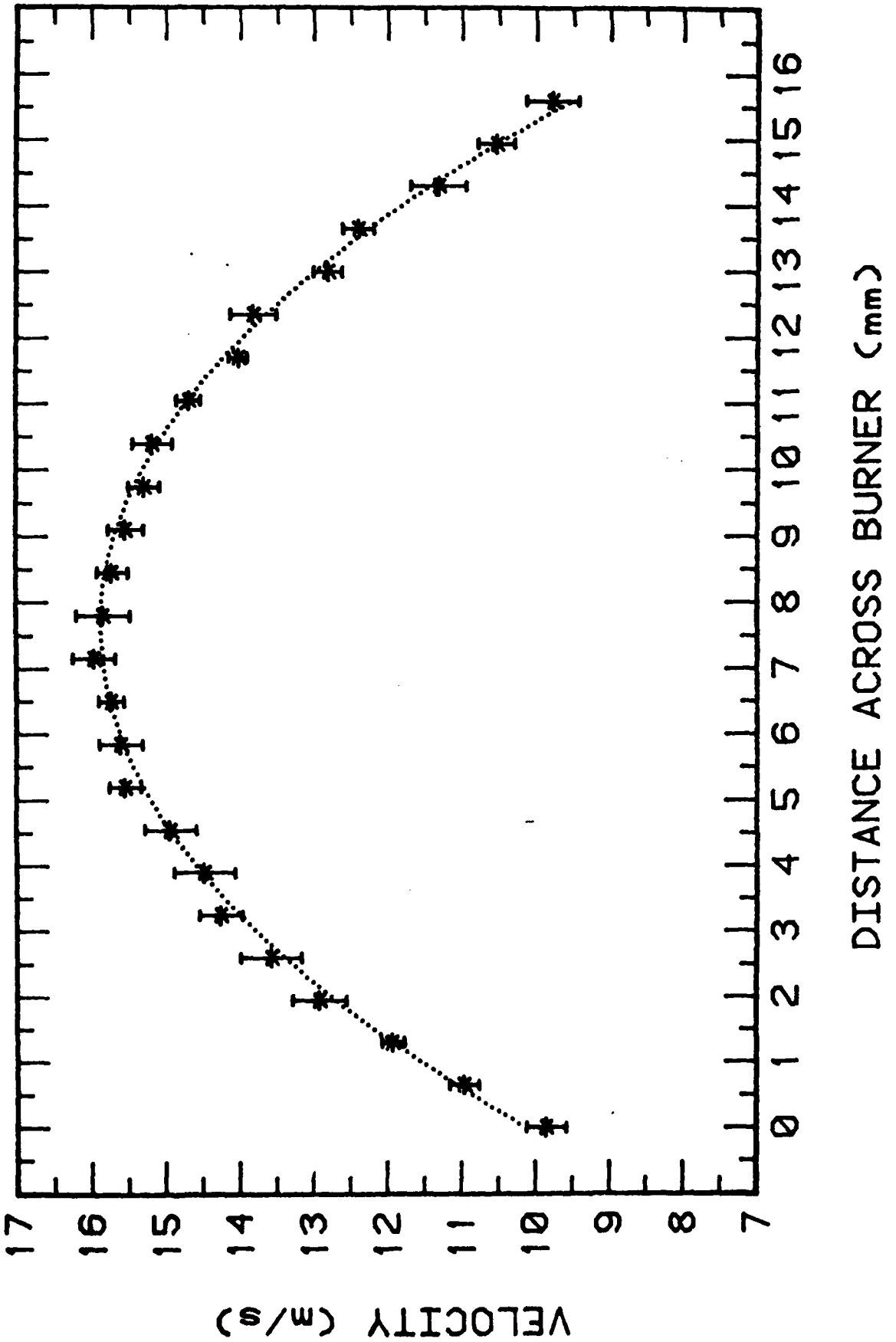
VELOCITY (m/s)
17
16
15
14
13
12
11
10
9
8
7
0 1 2 3 4 5 6 7 8 9 10 11 12 13 14 15 16
DISTANCE ACROSS BURNER (mm)

Fig. 2

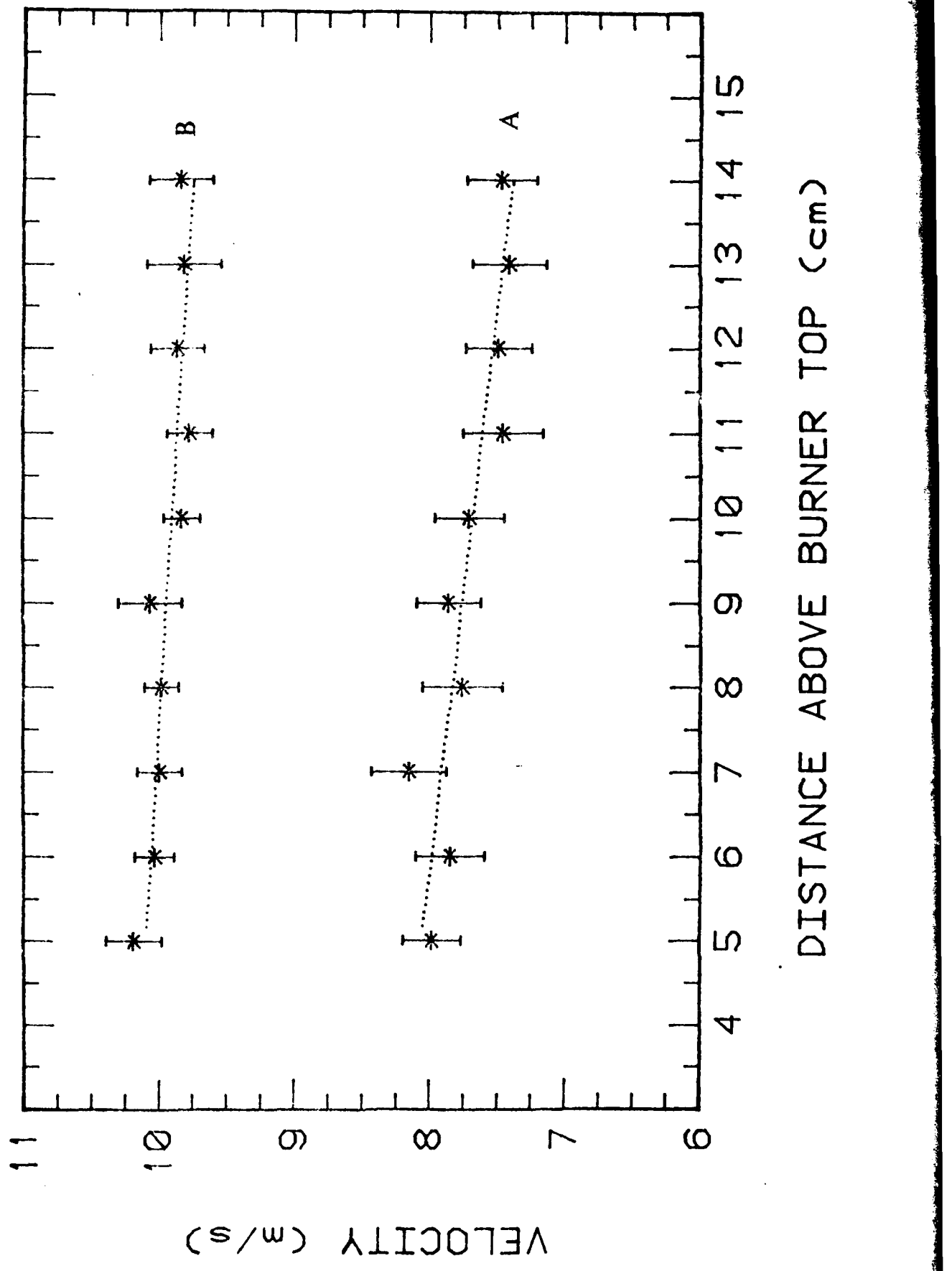
VELOCITY (m/s)
11
10
9
8
7
6
B
A
4
5
6
7
8
9
10
11
12
13
14
15
DISTANCE ABOVE BURNER TOP (cm)

Fig. 3

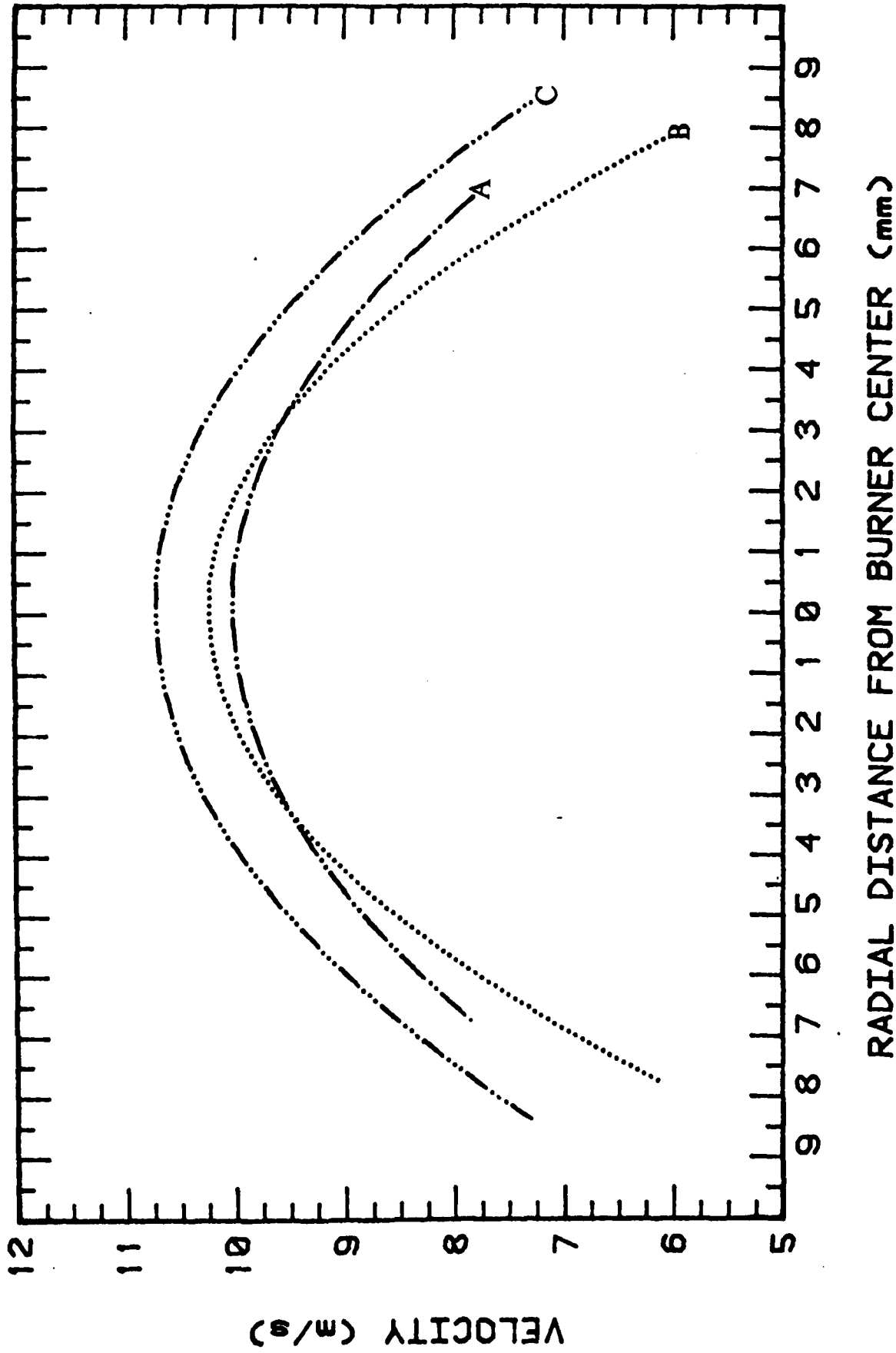
VELOCITY (m/s)
12
11
10
9
8
7
6
5
RADIAL DISTANCE FROM BURNER CENTER (mm)
9 8 7 6 5 4 3 2 1 0 1 2 3 4 5 6 7 8 9
A
B
C

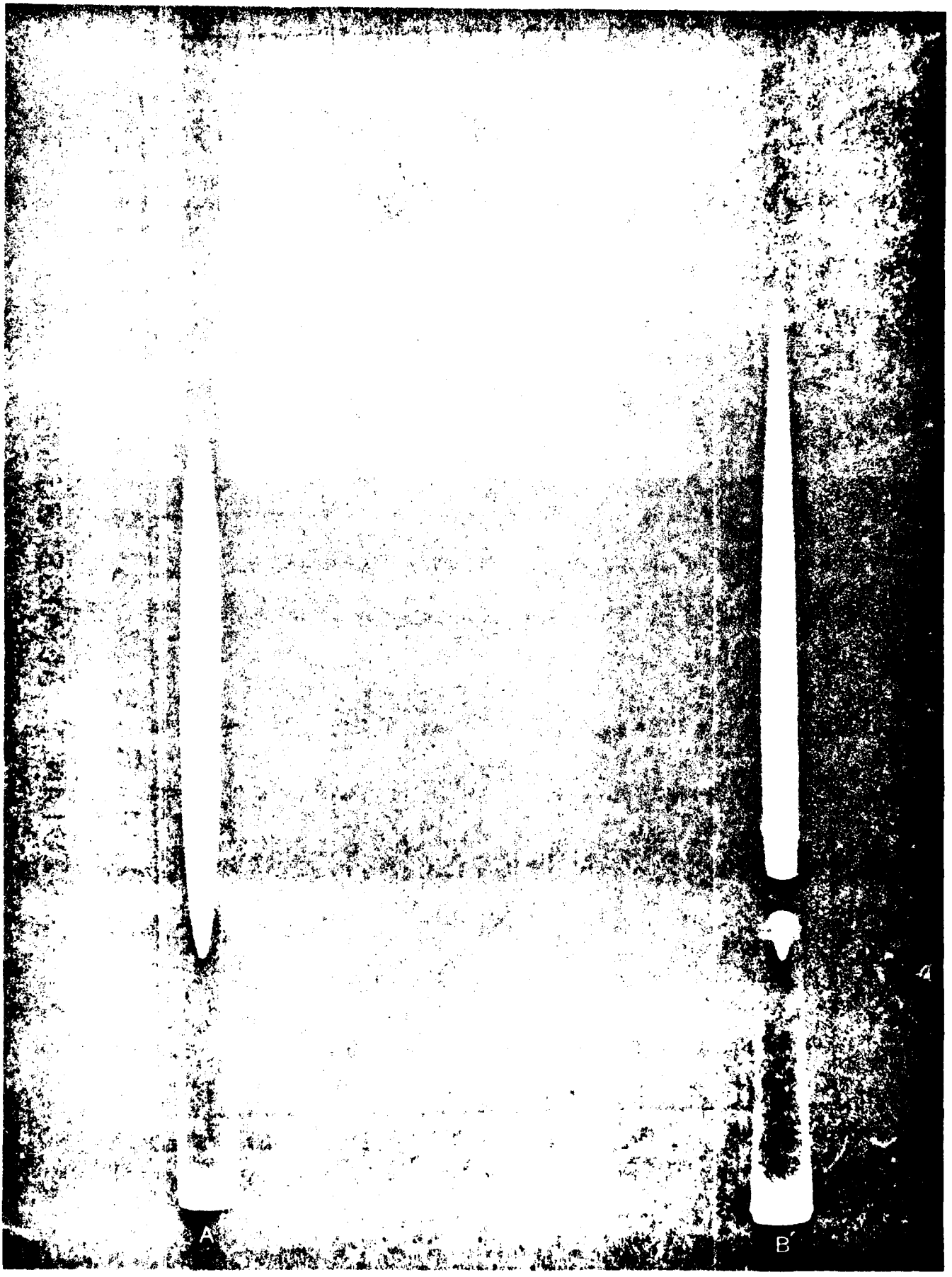
A
B´

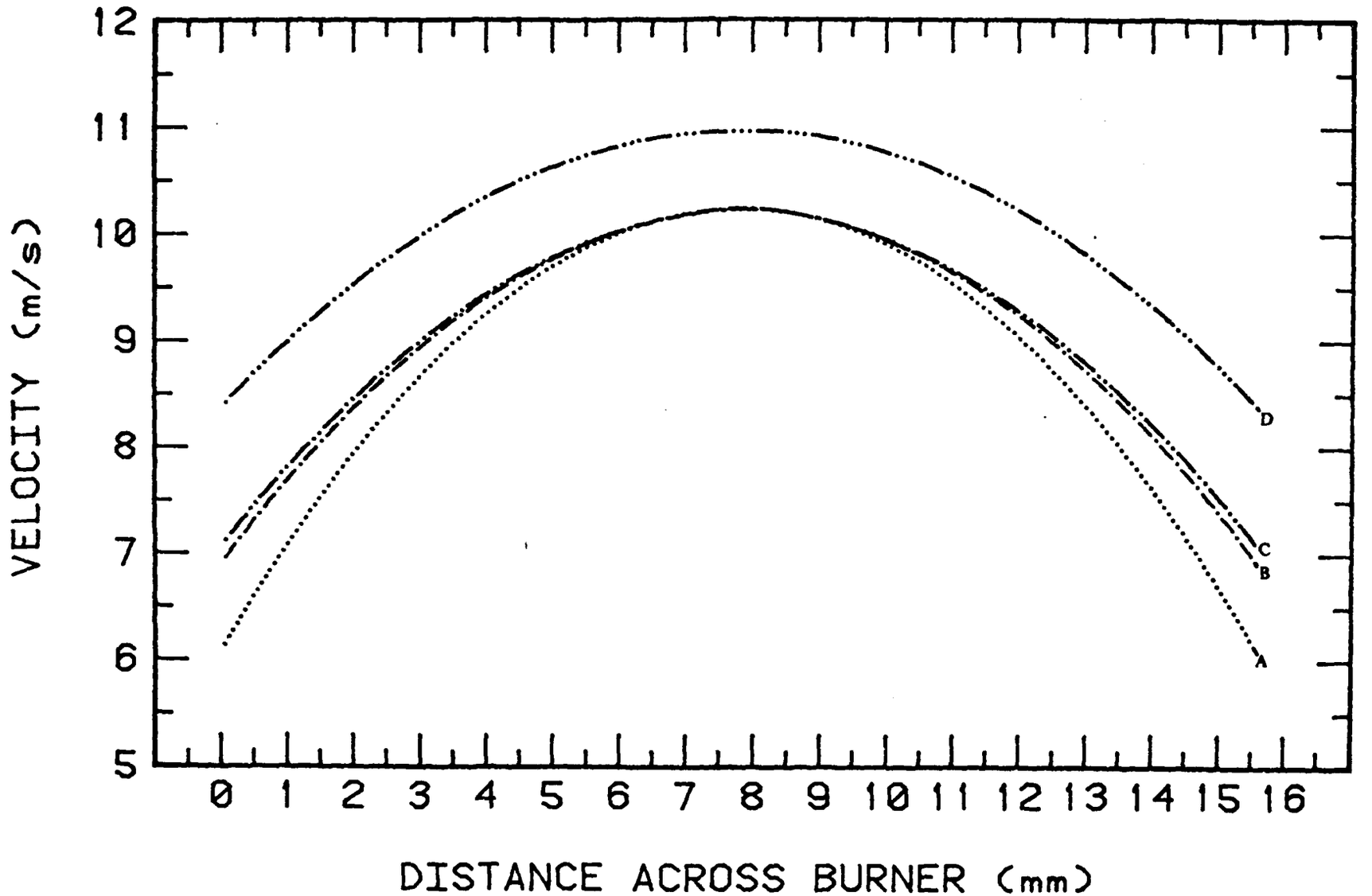
VELOCITY (m/s)
12
11
10
9
8
7
6
5
0 1 2 3 4 5 6 7 8 9 10 11 12 13 14 15 16
DISTANCE ACROSS BURNER (mm)
D
C
B
A

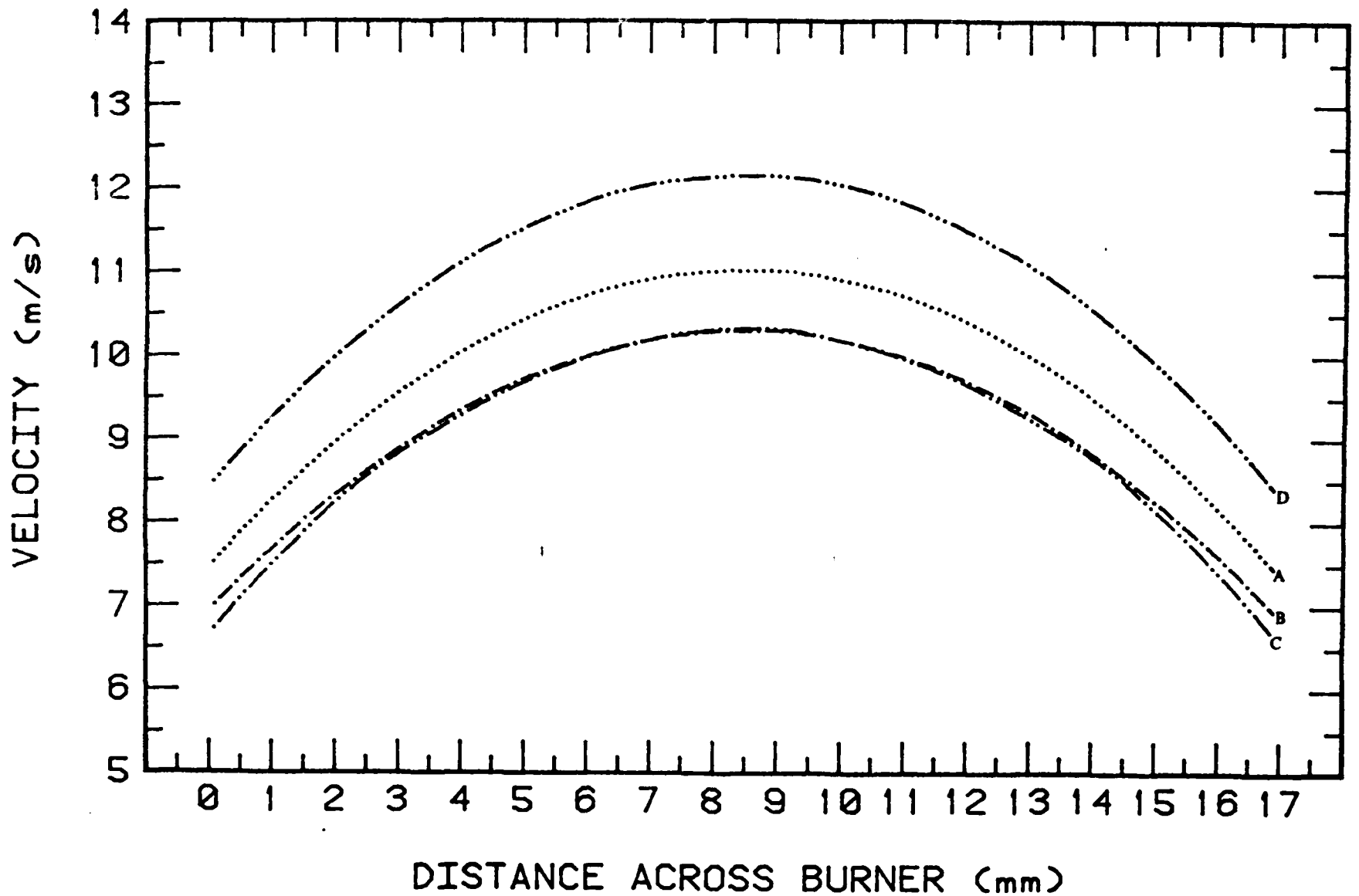
VELOCITY (m/s)
14
13
12
11
10
9
8
7
6
5
0 1 2 3 4 5 6 7 8 9 10 11 12 13 14 15 16 17
DISTANCE ACROSS BURNER (mm)
D
A
B
C

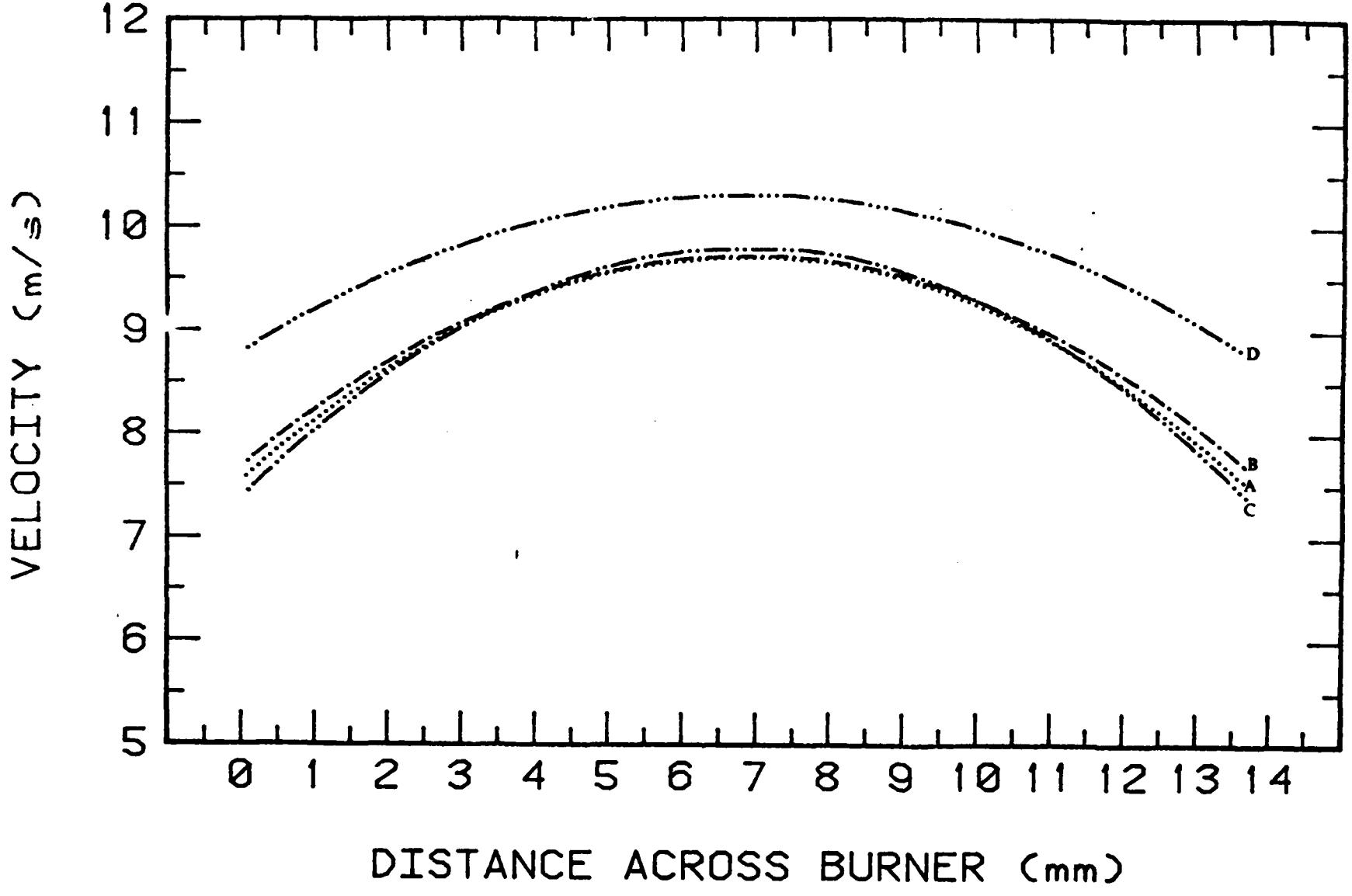
VELOCITY (m/s)
12
11
10
9
8
7
6
5
0 1 2 3 4 5 6 7 8 9 10 11 12 13 14
DISTANCE ACROSS BURNER (mm)
D
B
A
C

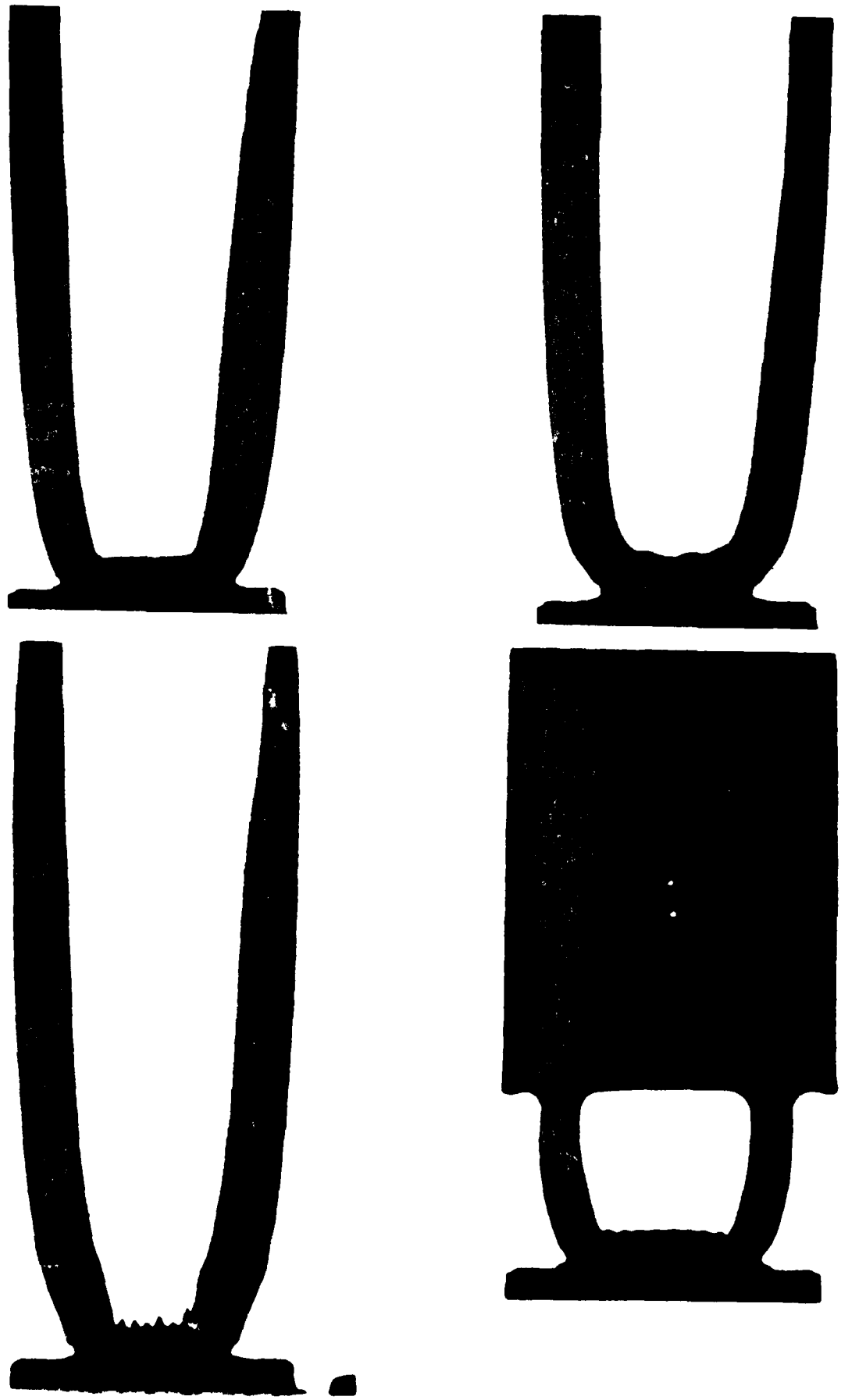

TECHNICAL REPORT DISTRIBUTION LIST, GEN

	No. Copies
Office of Naval Research Attn: Code 472 800 North Quincy Street Arlington, Virginia 22217	2
ONR Branch Office Attn: Dr. George Sandoz 536 S. Clark Street Chicago, Illinois 60605	1
ONR Area Office Attn: Scientific Dept. 715 Broadway New York, New York 10003	1
ONR Western Regional Office 1030 East Green Street Pasadena, California 91106	1
ONR Eastern/Central Regional Office Attn: Dr. L. H. Peebles Building 114, Section D 666 Summer Street Boston, Massachusetts 02210	1
Director, Naval Research Laboratory Attn: Code 6100 Washington, D.C. 20390	1
The Assistant Secretary of the Navy (RE&S) Department of the Navy Room 4E736, Pentagon Washington, D.C. 20350	1
Commander, Naval Air Systems Command Attn: Code 310C (H. Rosenwasser) Department of the Navy Washington, D.C. 20360	1
Defense Technical Information Center Building 5, Cameron Station Alexandria, Virginia 22314	12
Dr. Fred Saalfeld Chemistry Division, Code 6100 Naval Research Laboratory Washington, D.C. 20375	1
U.S. Army Research Office Attn: CRD-AA-IP P.O. Box 1211 Research Triangle Park, N.C. 27709	1
Naval Ocean Systems Center Attn: Dr. Joe McCartney San Diego, California 92152	1
Naval Weapons Center Attn: Dr. A. B. Amster, Chemistry Division China Lake, California 93555	1
Naval Civil Engineering Laboratory Attn: Dr. R. W. Drisko Port Hueneme, California 93401	1
Department of Physics & Chemistry Naval Postgraduate School Monterey, California 93940	1
Dr. A. L. Slafkosky Scientific Advisor Commandant of the Marine Corps (Code RD-1) Washington, D.C. 20380	1
Office of Naval Research Attn: Dr. Richard S. Miller 800 N. Quincy Street Arlington, Virginia 22217	1
Naval Ship Research and Development Center Attn: Dr. G. Bosmajian, Applied Chemistry Division Annapolis, Maryland 21401	1
Naval Ocean Systems Center Attn: Dr. S. Yamamoto, Marine Sciences Division San Diego, California 91232	1
Mr. John Boyle Materials Branch Naval Ship Engineering Center Philadelphia, Pennsylvania 19112	1

TECHNICAL REPORT DISTRIBUTION LIST, 051C

	No. Copies
Dr. M. L. Denton Department of Chemistry University of Arizona Tucson, Arizona 85721	1
Dr. K. A. Osteryoung Department of Chemistry State University of New York at Buffalo Buffalo, New York 14214	1
Dr. L. R. Kowalski Department of Chemistry University of Washington Seattle, Washington 98105	1
Dr. S. P. Perone Department of Chemistry Purdue University Lafayette, Indiana 47907	1
Dr. D. L. Venezky Naval Research Laboratory Code 6130 Washington, D.C. 20375	1
Dr. H. Freiser Department of Chemistry University of Arizona Tucson, Arizona 85721	
Dr. Fred Saalfeld Naval Research Laboratory Code 6110 Washington, D.C. 20375	1
Dr. P. Chernoff Department of Mathematics Massachusetts Institute of Technology Cambridge, Massachusetts 02139	1
Dr. E. Wilson Department of Chemistry University of California, San Diego La Jolla, California	1
Dr. A. Zirino Naval Undersea Center San Diego, California 92132	1
Dr. John Duffin United States Naval Postgraduate School Monterey, California 93940	1
Dr. G. M. Hieftje Department of Chemistry Indiana University Bloomington, Indiana 47401	1
Dr. Victor L. Rehn Naval Weapons Center Code 3813 China Lake, California 93555	1
Dr. Christie G. Enke Michigan State University Department of Chemistry East Lansing, Michigan 48824	1
Dr. Kent Eisentraut, MBT Air Force Materials Laboratory Wright-Patterson AFB, Ohio 45433	1
Walter G. Cox, Code 3632 Naval Underwater Systems Center Building 148 Newport, Rhode Island 02840	1
Professor Isiah M. Warner Texas A&M University Department of Chemistry College Station, Texas 77840	1
Professor George H. Morrison Cornell University Department of Chemisty Ithaca, New York 14853	1
Dr. Rudolph J. Marcus Office of Naval Research Scientific Liaison Group American Embassy APO San Francisco 96503	1
Mr. James Kelley DTNSRDC Code 2803 Annapolis, Maryland 21402	1